

Reconstructions of Computed-Tomography Imaging Spectrometer Image Cubes Using Calculated System Matrices

Daniel W. Wilson, Paul D. Maker, and Richard E. Muller

Jet Propulsion Laboratory
California Institute of Technology
Pasadena, CA 91109

ABSTRACT

The computed-tomography imaging spectrometer (CTIS) captures a scene's spatial and spectral information without any type of scanning. This capability enables a variety of applications that require spectral imaging of transient events. In this work, we demonstrate a flexible CTIS calibration technique that allows multiple scene resolutions to be reconstructed from a single detector frame. The technique combines measurements with simulations to determine the transfer matrix of the system. Reconstructions of an experimental scene are performed to demonstrate the flexibility of the approach.

1. INTRODUCTION

There are a number of applications in defense, remote-sensing, and medicine where spectral imaging of transient scenes would be useful. A candidate instrument for performing such transient-event spectral imaging is the **computed-tomography imaging spectrometer (CTIS)**.¹⁻⁷ This type of imaging spectrometer is unique in that it can capture a scene's spatial and spectral information without any type of scanning. Other types of imaging spectrometers perform either spatial scanning or spectral scanning which results in data corruption for transient scenes. **CTIS** avoids the need for scanning by utilizing a two-dimensional grating that splits the scene into multiple spectrally-dispersed images that are captured by a focal plane array (**FPA**). The intensity data from a single FPA snapshot is then processed using computed-tomography algorithms to reconstruct the scene into a cube of spatial (position x and y) and spectral (wavelength λ) information. In this paper, we describe how we calibrate our system by combining a small number of measurements with a ray-tracing simulation. We then use the resulting calibration data to reconstruct multiple spatial-spectral data cubes of differing resolution from a single experimental **FPA** image.

2. EXPERIMENTAL SYSTEM

An illustration of our experimental system is shown in Fig. 1 and has a layout similar to that of Descour et al.^{5,7} The primary lens is a 35-80 mm zoom, the field stop is a 4.5 mm square aperture, the collimating lens is a 70-210 mm zoom (set at 210 mm, $f/5.6$, focused at infinity), and the **re-imaging** lens is 50 mm lens ($f/5.6$ focused at infinity). All lenses were commercial 35 mm camera lenses. The camera is a Kodak **Megaplug 1.6i** (1528x 1024 9 μm pixels, 10-bit digital). There are two interference filters in the collimated region of the optical system, a long-wave pass with cut-on wavelength of 450 nm and a short-wave pass with cut-off wavelength of 770 nm. Together they define the band-pass of the system to be 450-770 nm.

The two-dimensional grating is specially designed to produce high-efficiency diffraction into a 5x5 array of orders. The grating is actually an array of computer generated hologram (**CGH**) cells composed of 8x8 2.4 μm pixels. The resulting grating has a period of 19.2 μm and fills an area 1.7 cm in diameter. The **CGH** was designed so that the 5x5 array of orders had relative efficiencies of 1.5, 1.2, 1 for orders $\pm 2, \pm 1, 0$, respectively. This efficiency grading provides nearly uniform signal intensity over the **FPA** for a spatially and spectrally uniform (white) scene (due to increased dispersion of the higher orders). The desired wavelength range was 450-770 nm, so the design wavelength for the **CGH** was chosen to be 590 nm.

Further author information -

D.W.W. (correspondence): Email: dwilson@vaxeb.jpl.nasa.gov; Telephone: 818-393-3548; Fax: 818-393-4540

Because there are many possible CGH designs that produce the desired 5x5 efficiency pattern at the design wavelength, we performed many designs and chose the one that had the best simulated broadband performance.’ The grating is fabricated in **poly-methylmethacrylate** by analog direct-write electron-beam lithography followed by development in pure acetone. A detailed description of our CGH fabrication procedure can be found in Refs. 8 and 9.

3. CALCULATION OF SYSTEM MATRICES

The mathematical representation of a CTIS system has been described by Descour et al.^{5,6} The system can be represented by the equation

$$\mathbf{g} = \mathbf{H}\mathbf{f} + \mathbf{n}, \quad (1)$$

where \mathbf{g} is a $N_d \times 1$ vector of detector intensities (x, y mapped to $d = 1 \dots N_d$), \mathbf{H} is a $N_d \times N_s$ sparse matrix of **scene-voxel** to detector-pixel connection strengths, \mathbf{f} is a $N_s \times 1$ vector of scene **voxel** intensities (x, y, λ mapped to $s = 1 \dots N_s$), and \mathbf{n} is a vector of random noise which we will ignore for this analysis. To reconstruct an unknown scene \mathbf{f} from a measured detector image \mathbf{g} , we have to effectively invert equation Eq. (1). Hence the system matrix \mathbf{H} must be known accurately. Each column s of the matrix contains the connection weights of scene **voxel** f_s to all of the detector pixels. To determine (calibrate) these weights and fill the matrix, one can (1) measure the **weights**⁵, (2) simulate the system and calculate the weights, or (3) combine measured data with simulation to determine the weights. The first option, measurement, is hardware intensive and time consuming because the setup must be adjusted to address each **voxel** in spatial-spectral space, and data from all **voxels** must be recorded and assembled into the system matrix. The second option, pure simulation, is error prone because of the number of complex components in the system—each lens and filter has its own spectral transmission function, as do each of the grating orders. We have implemented the third option, combined measurement and simulation.

The measurement portion of the procedure involves **determining** the system efficiency (field stop to detector) for **one position** in the field stop, in all diffraction orders, at wavelengths throughout the bandpass of the **system**. **First**, a **calibrated** optical power meter is used to measure the output of a 50 μm core fiber that has been illuminated by a **monochrometer**. The fiber is then positioned in the center of the field stop, and images are captured at each wavelength (450 nm -770 nm in 10 nm steps). These images are processed by a computer program that finds the **centroids** of the diffraction orders and sums the counts in each order. The order-count sums are converted to relative efficiencies using the measured fiber output powers and the camera settings (shutter speed and gain) used to capture the image. The order centroids are used to derive the effective focal length of there-imaging lens plus camera window (we assume that grating period of 19.2 μm is **correct** due to the high accuracy of the electron-beam lithography).

With the efficiencies of **all** the orders known, we then use simulation to derive the transfer matrix \mathbf{H} that maps **voxels** in the **field** stop to pixels on the detector. This is accomplished by tracing many rays through the system and keeping track of the resulting **scene-voxel** to detector-pixel connection weights. Starting from random positions (x, y, λ) within each **voxel**, each ray is traced through the collimating lens, grating, and **re-imaging** lens to the detector. In this experiment, the lenses were modeled as ideal point-source to plane-wave transformers (or vice-versa). Even though aberrations will cause deviation from this model, commercial camera lenses are well corrected and should perform well over the FPA area which is much smaller than a 35 mm film frame. At the grating, a single ray [plane wave] is diffracted into multiple orders. The incident wave vector \mathbf{k}_{inc} is derived from the scene **voxel**'s position and wavelength, and the diffracted wave vector \mathbf{k}_{diff} is determined by the Floquet condition, $k_{\text{diff},x} = k_{\text{inc},x} - m_x K_x, k_{\text{diff},y} = k_{\text{inc},y} - m_y K_y, k_{\text{diff},z} = [k_0^2 - k_x^2 - k_y^2]^{1/2}$, where $m_x, m_y = 0, \pm 1, \pm 2, \pm 3$ are order indices, K_x, K_y are the grating vectors ($K_{x,y} = 2\pi/\Lambda_{x,y}$, where $\Lambda_{x,y}$ is the grating period = 19.2 μm), and $k_0 = 2\pi/\lambda$. The diffracted rays are assigned weights in accordance with the measured order efficiencies and the scene volume that they represent. Efficiencies for wavelengths between those measured are found by interpolation. Finally, the rays are traced through the **re-imaging** lens to the detector, where the pixel locations are determined. The detector pixel values are stored as a column of \mathbf{H} after a sufficiently large number of rays have been traced from a given **voxel** to produce a smooth, noiseless **FPA** response. Typically 50 rays/mm \times 50 rays/mm (spatial density) \times 500 rays/ μm (spectral density) from randomly chosen positions within the **voxel** are required. This procedure is repeated for all the **voxels** in the scene.

4. RECONSTRUCTION ALGORITHM

Following Descour et al.^{4,5}, we use the expectation-maximization (EM) algorithm to reconstruct unknown scenes from measured detector matrices. This algorithm was developed for reconstructing positron-emission tomography medical images.]” The reconstruction is started with an initial guess for the scene, and then a predicted detector vector is calculated,

$$\mathbf{g}_{\text{pred}} = \mathbf{H} \mathbf{f}. \quad (2)$$

Corrections are then made to the scene based on the back projection of the ratio of the measured detector and predicted detector,

$$f'_s = f_s \left(\frac{1}{\sum_d H_{d,s}} \right) \left[\mathbf{H}^T \begin{pmatrix} \mathbf{g}_{\text{meas}} \\ \mathbf{g}_{\text{pred}} \end{pmatrix} \right]_s, \quad s = 1 \dots N_s \quad (3)$$

where the ratio of the \mathbf{g} vectors is performed element by element. If $\mathbf{g}_{\text{meas}} = \mathbf{g}_{\text{pred}}$, then the second factor becomes the inverse of the first and there is no change to \mathbf{f} . Equations (2) and (3) are used iteratively until the predicted detector matches the measured detector to a desired error tolerance or until the improvement stagnates. We have achieved best results when we start with an initial guess of unity for all voxels. Typically 10-30 iterations are required for acceptable scene reconstructions. It is known that images reconstructed using EM can develop edge effects and noise as the iterations proceed. Researchers in the positron-emission tomography community have developed a number of techniques to suppress such degrading effects.¹¹ In this work we have not implemented any such improvements.

5. EXPERIMENTAL RESULTS

Our experimental scene consists of a circuit board with several light-emitting diodes (LEDs) and various laser spots as shown in Fig. 2. The goal is to investigate to what extent multiple scene resolutions can be reconstructed from a single captured CTIS image. Figure 3a shows a full-resolution 1528x1024 pixel image of the scene, and Fig. 3b shows the result of binning the central 1024x1024 down to 256x256 (blocks of 4x4 pixels summed). The inset shows the resolution of the zeroth order image. The 256x256 image was reconstructed into spatial-spectral scenes having the a wide variety of resolutions ($N_x \times N_y \times N_\lambda$) as summarized in Table I. For each resolution, the system matrix size, nonzero density, and the memory requirement are given. All reconstructions were performed with 20 iterations of the EM algorithm operating on the same data set. The times shown are for a 200 MHz Pentium Pro with 128 MB of RAM. The normalized error is the root-mean-square (rms) detector error normalized by the maximum of the measured detector: $\text{rms}(\mathbf{g}_{\text{pred}} - \mathbf{g}_{\text{meas}}) / \max(\mathbf{g}_{\text{meas}})$. A number of observations can be made about the data in Table I. For nearly all of the system matrices, the nonzero density was less than 1 % and it decreased slightly with increasing spectral resolution. The storage requirements for the matrices were quite large and ultimately limited the total reconstruction resolution because we desired that disk caching be avoided. As for the reconstructions, note that as the spatial resolution increases, the normalized error decreases. This is because low spatial resolution reconstructions cannot accurately represent the highly structured experimental scene. Figure 4 shows the reconstruction results for $N_x \times N_y \times N_\lambda = 16 \times 16 \times 32, 32 \times 32 \times 32, 32 \times 32 \times 48, \text{ and } 40 \times 40 \times 32$. The images on the left side of the figure show the reconstructed scenes with the gray level proportional to the intensity integrated over all wavelengths. The plots on the right side of the figure show the spectra of the marked pixels. Note that in all cases the 594 nm and 633 nm laser spots reconstructed into the proper spectral bands. Figure 5 shows the reconstruction into 40x40 spatial resolution by 8 unequal width spectral bands. This example shows that if an application requires differing resolution throughout the spectrum, then it can be achieved with minimum computational effort. Note that the narrowest band is 10 nm wide (equal to the 40x40x32 example), but the matrix is smaller and the reconstruction is faster. In fact, neither the spatial nor the spectral dimensions of the voxels need to be equal. Finally, Fig. 6 shows the 64x64x3 reconstruction. This demonstrates that increased spatial resolution can be achieved at the expense of spectral resolution. Note that in all of the reconstructions having spatial resolution higher than 32x32, the panchromatic image has clearer features than the central order image on the 256x256 detector (inset of Fig. 3b). This indicates that the calibration is accurate enough to allow the EM algorithm to utilize the information in the higher diffraction orders for extrapolation to higher spatial resolution.

Table 1. CTIS System Matrix Calculations and Image Reconstructions

System Parameters: Field stop size = 4.5 mm, $f_1 = 210$ mm, $f_2 = 51.64$ mm, 2D Grating period= 19.2 μm
 Detector size: 9.216x9.216 mm, 1024x1024 9-pm pixels binned 4x4 to 256x256 36- μm pixels

Scene Resolution $N_x \times N_y \times N_z$ (450-770 nm)	Matrix Size	Non zero Density	Storage (MB)	EM Time (see) (20 iterations)	Normalized Error
16X16X16	65536x4096	0.92 %	18.9	10.7	0.0112
16x1 6x32	65536x8 192	0.64 %	26.3	15.0	0.0103
16x16x48	65536x12288	0.55 %	33.7	18.9	0.0103
32x32x16	65536x16384	0.51 %	41.8	22.5	0.0071
32x32x32	65536x32768	0.33 %	54.1	29.2	0.0042
32x32x48	65536x49152	0.27 %	66.0	36.1	0.0041
40x40x32	65536x51200	0.28 %	72.0	37.6	0.0035
64x64x3	65536x12288	1.49 %	91.3	1957 (disk cached)	0.0336
40x40x8 unequal bands	65536x8192	0.75 %	48.2	25.4	0.0109

6. CONCLUSION

We have demonstrated that computed-tomography imaging spectrometers can be calibrated with a combined measurement-simulation procedure. The result is a flexible system that can be used to reconstruct scenes of variable resolutions from a single detected image. Future experiments will compare CTIS reconstructions to spectra from calibrated point spectrometers and calibrated reflectance targets. Results from such experiments will help determine if CTIS systems can be accurate enough for practical applications.

ACKNOWLEDGMENTS

The research described in this paper was performed by the Center for Space Microelectronics Technology, Jet Propulsion Laboratory, California Institute of Technology, and was jointly sponsored by the Ballistic Missile Defense Organization/Innovative Science and Technology Office, NASA Office of Space Science, and the Caltech President's Fund, through and agreement with the National Aeronautics and Space Administration. We would also like to thank Prof. Michael Descour of University of Arizona and Gregory Bearman of JPL for helpful discussions.

REFERENCES

1. T. Okamoto, I. Yamaguchi, "Simultaneous acquisition of spectral image information," *Opt. Lett.*, **16**, no. 16, pp. 1277-1279 (1991).
2. T. Okamoto, A. Takahashi, I. Yamaguchi, "Simultaneous acquisition of spectral and spatial intensity distribution," *Appl. Spectroscopy*, **47**, no. 8, pp. 1198-1202 (1993).
3. F. V. Bulygin, G. N. Vishnyakov, G. G. Levin, and D. V. Karpukhin, "Spectrotomography-a new method of obtaining spectrograms of 2-D objects," *Opt. Spectroscopy (USSR)*, **71**, pp.56 1-563 (1991).
4. M. R. Descour, Non-scanning Imaging Spectrometry, Ph.D Dissertation, University of Arizona (1994).
5. M. R. Descour and E. L. Dereniak, "Computed-tomography imaging spectrometer: experimental calibration and reconstruction results," *Appl. Opt.*, **34**, no. 22, pp. 4817-4826 (1995).
6. M. R. Descour, R. Schowengerdt, and E. L. Dereniak, "Analysis of the computed-tomography imaging spectrometer by singular value decomposition," in *Algorithms for Multispectral and Hyperspectral Imagery II*, E. Iverson, ed., SPIE 2758-46, pp. 127-133 (1996).
7. M. R. Descour, C. E. Volin, T. M. Gleeson, E. L. Dereniak, M. F. Hopkins, D. W. Wilson, and P. D. Maker, "Demonstration of a computed-tomography imaging spectrometer using a computer-generated hologram disperser," *Appl. Opt.*, **36**(16), pp. 3694-3698 (Jun 1, 1997).

8. P. D. Maker and R. E. Muller, "Phase holograms in poly-methylmethacrylate," *J. Vat. Sci. Technol. B*, **10**, pp. 2516-2519 (1992).
9. P. D. Maker, D. W. Wilson, and R. E. Muller, "Fabrication and performance of optical interconnect analog phase holograms made by electron-beam lithography," in *Optoelectronic interconnects and Packaging*, R. T. Chen and P. S. Guilfoyle, eds., SPIE vol. CR62, pp. 415-430 (1996).
10. L. A. Shepp and Y. Vardi, "Maximum likelihood reconstruction for emission tomography," *IEEE Trans. Med. Imag.*, **MI-1**, no. 2, pp 113-122 (1982).
11. D. L. Snyder, M. I. Miller, L. J. Thomas, Jr., and D. G. Politte, "Noise and edge artifacts in maximum-likelihood reconstructions for emission tomography," *IEEE Trans. Med. Imag.*, **MI-6**, no. 3, pp. 228-238, Sept. 1987.

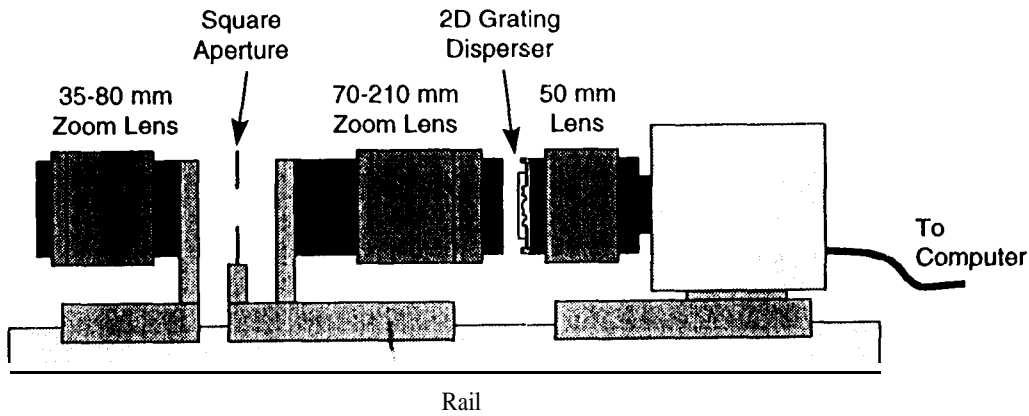


Figure 1. Illustration of experimental CTIS system. All lenses are commercial 35 mm camera lenses, and the camera is a 1534x1024 9-pm pixel CCD (10-bit).

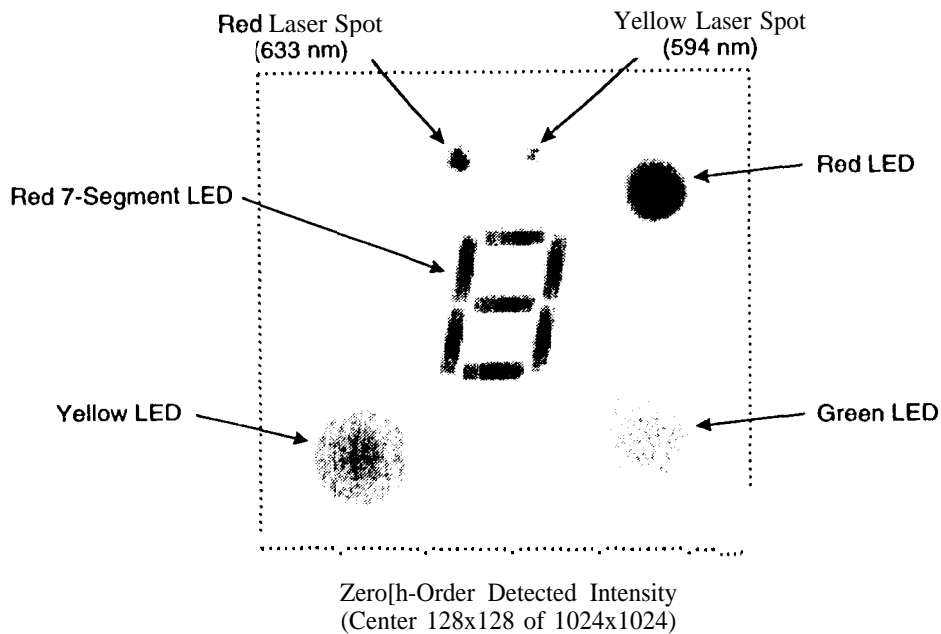


Figure 2. Zeroth-order image of the experimental scene composed of light-emitting diodes and two laser spots on a circuit board.

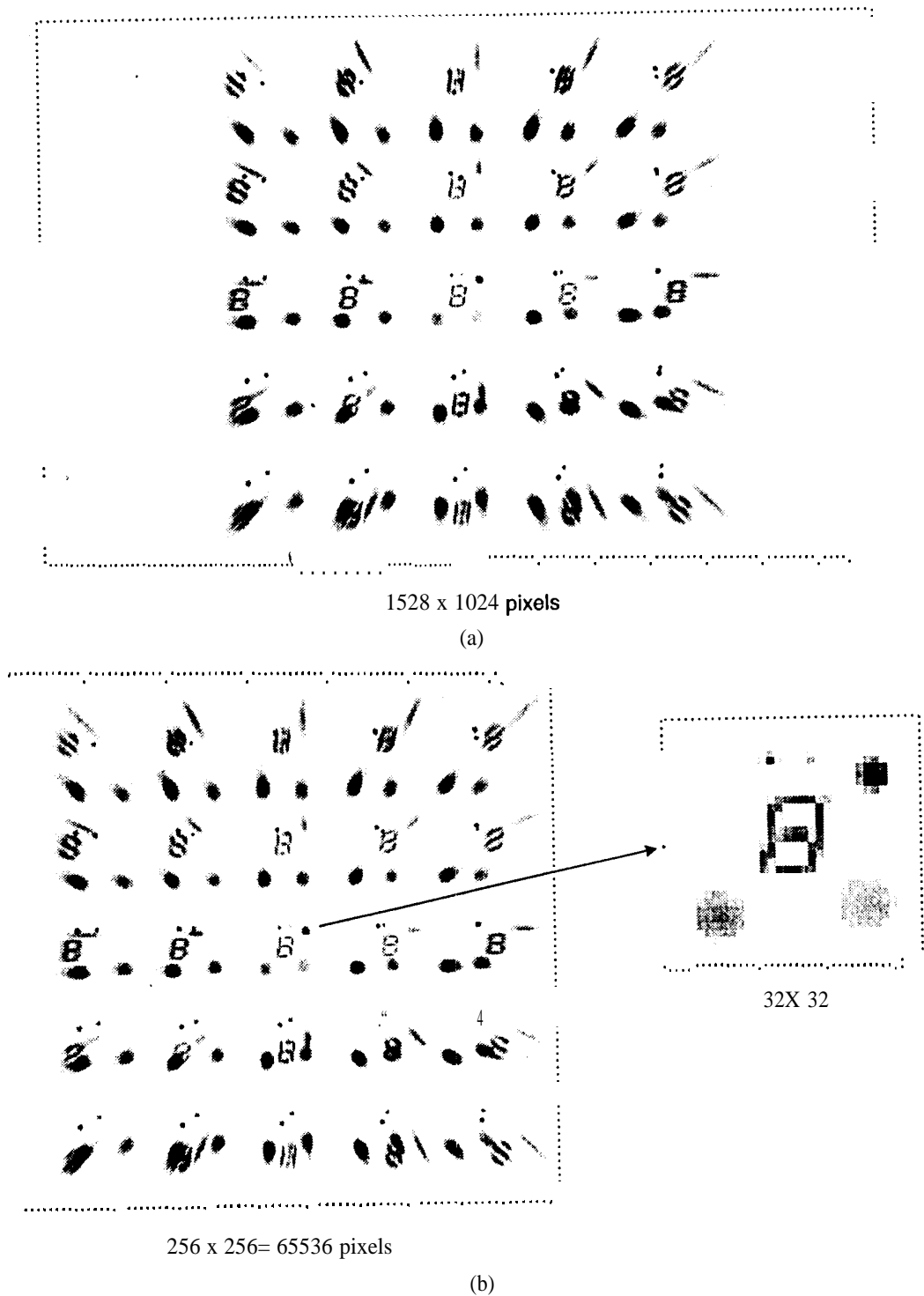


Figure 3. Detected image of the experimental scene. (a) Full resolution. (b) Result of binning central 1024x1024 of full-resolution image 4x4 pixels at a time down to 256x256. This image was used as the detector for all reconstructions. Inset shows zeroth order resolution.

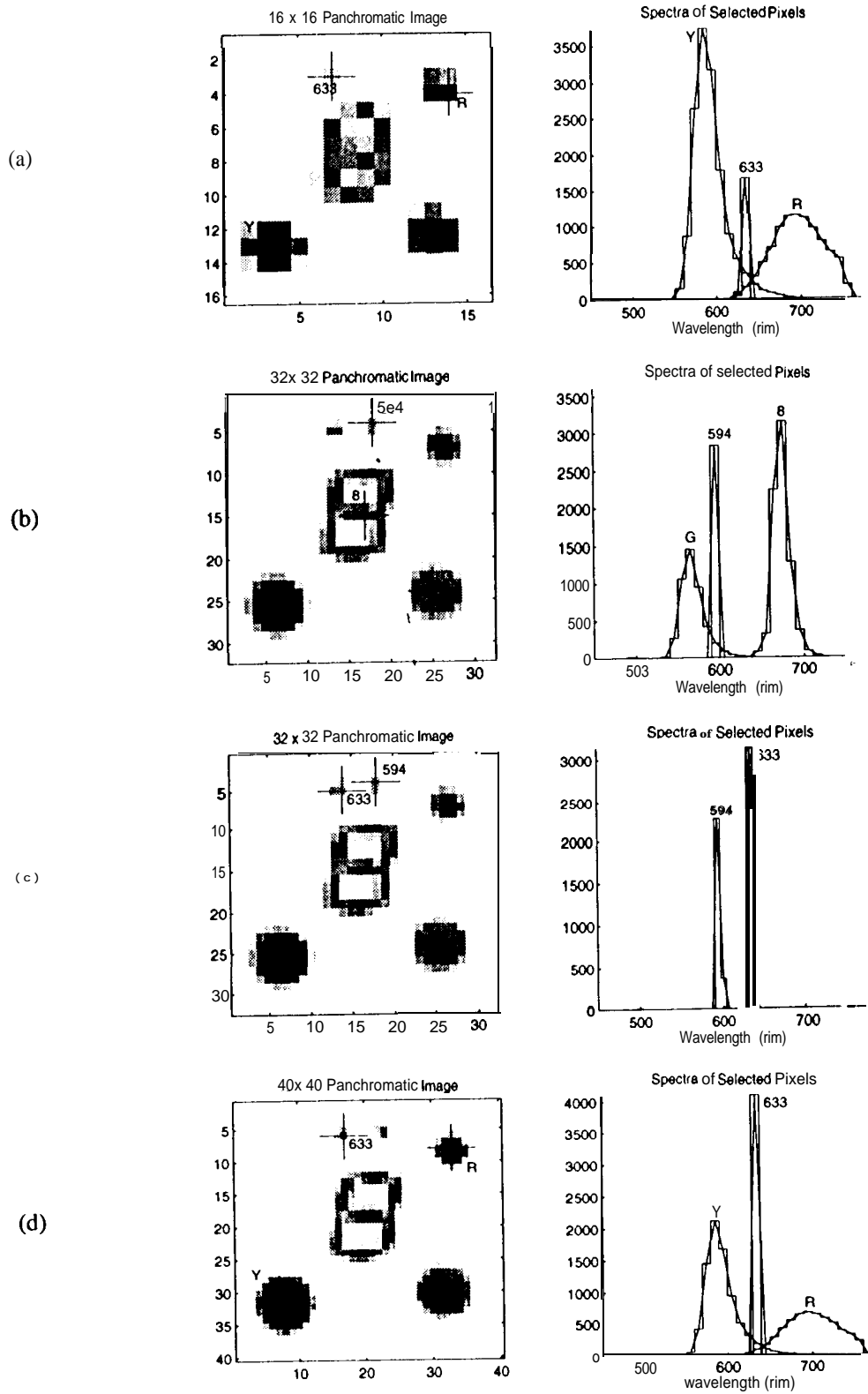


Figure 4. Reconstructed scenes from the 256x256 detector image in Fig. 3b. (a) 16x16x32, (b) 32x32x32, (c) 32x32x48, (d) 40x40x32.

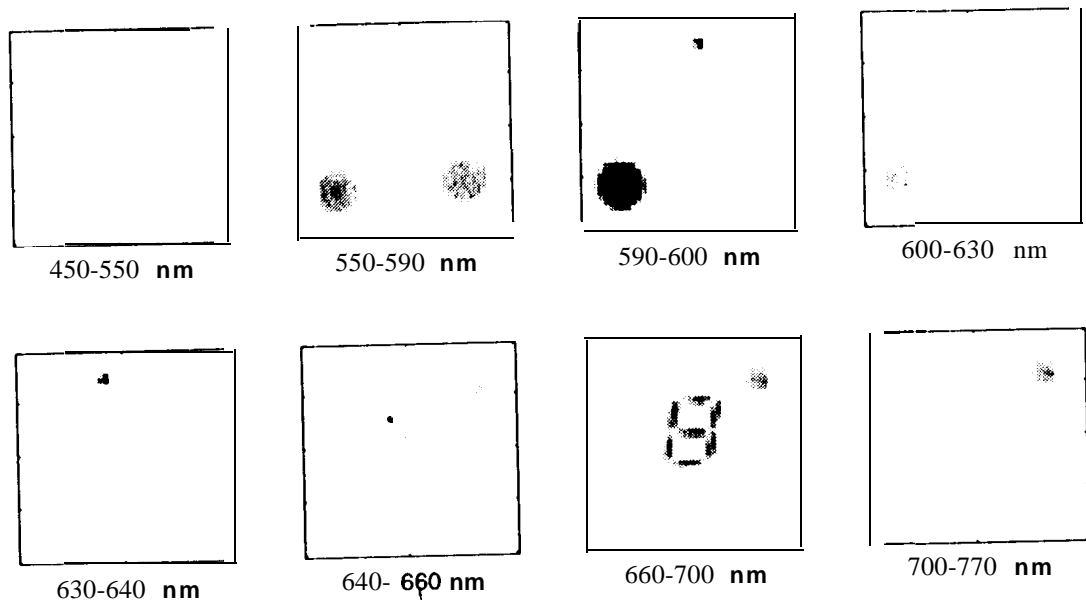


Figure 5. Reconstruction of detector image in Fig. 3b into a scene having 40x40x8 voxels where the spectral bands have unequal widths.

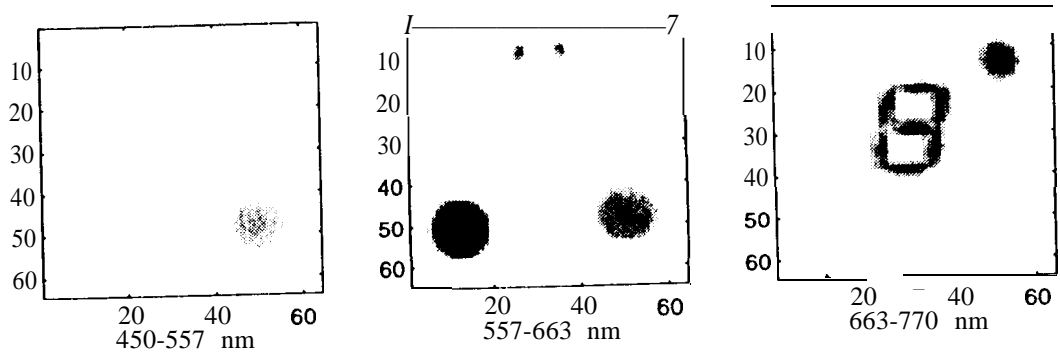


Figure 6. Reconstruction of detector image in Fig. 3b into a scene having 64x64x3 voxels.



***Reconstructions of Computed-Tomography Imaging Spectrometer
image Cubes Using
Calculated System Matrices***

Dan Wilson, Paul Maker, and Rich Muller

*Center for Space Microelectronics Technology
Jet Propulsion Laboratory
California Institute of Technology
Pasadena, CA 91109*

Funding:
BMDO/ 1ST, NASA, and
Caltech President's Fund (with M. Descour, UAZ)

Outline

1. Background
2. Experimental Setup
3. Calibration by Measurement and Simulation .
4. Reconstructions of an Experimental Target
5. Summary

Motivation

Desire: Perform *imaging spectrometry of transient events*

Defense

Missile launches

Target identification

Space Exploration

Fast flybys

Eruptions / impact explosions on planetary bodies

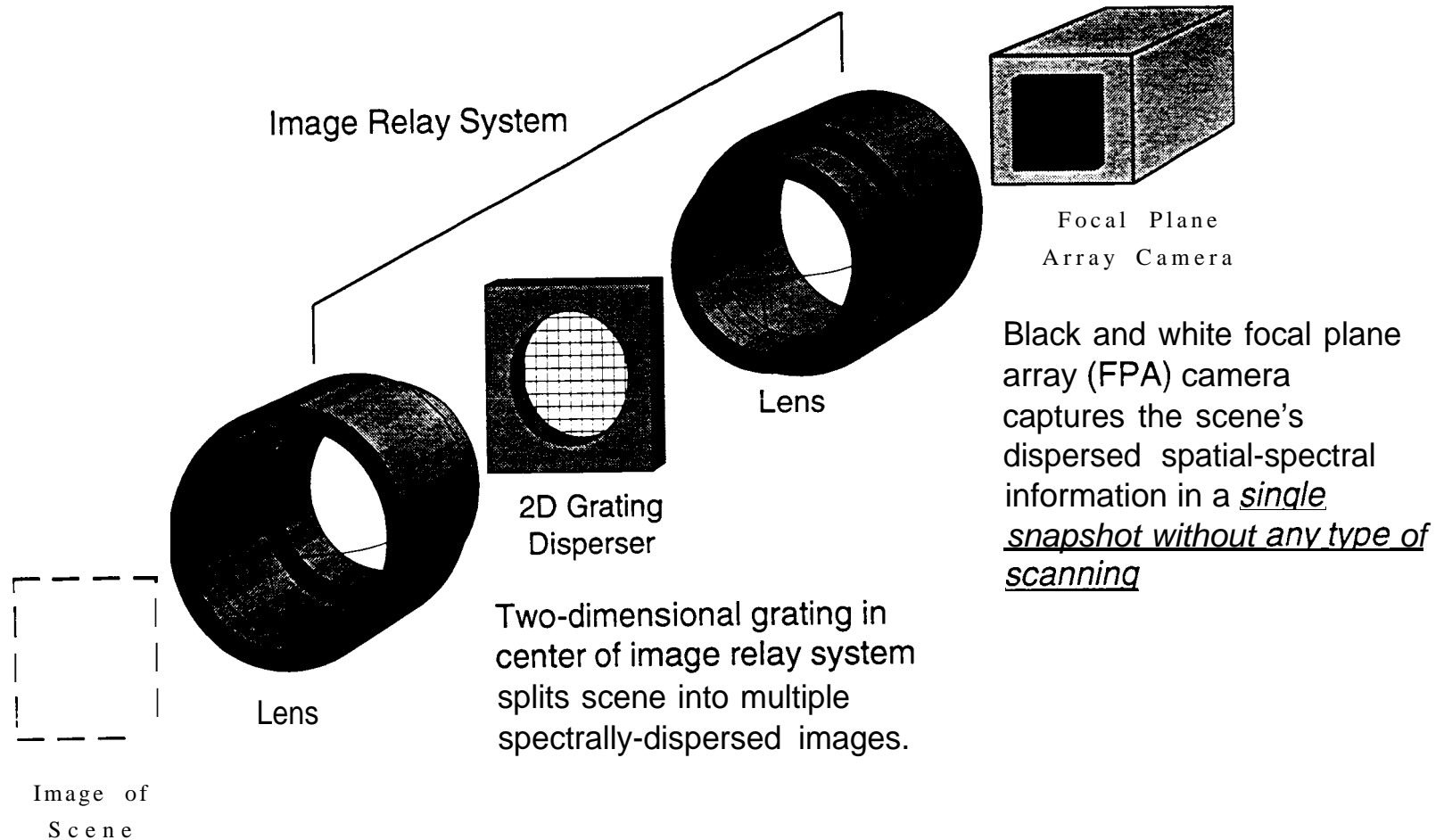
Problem: *Transient events cannot be captured* by traditional imaging spectrometers because they require some sort of *scanning*

Spatial scanning - narrow slice of image dispersed by grating

Spectral scanning - bandpass filtering of image

Objective: Investigate the *computed-tomography imaging spectrometer* (CTIS) concept as a solution for capturing transient events

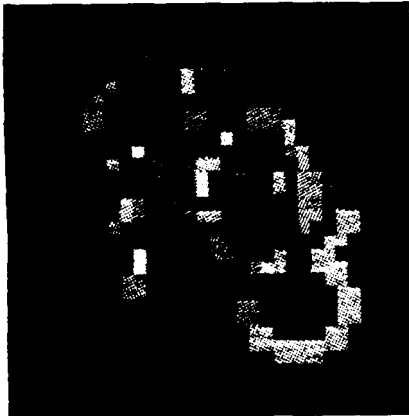
Principle of Operation



Primary imaging system (not shown) forms image of a scene.

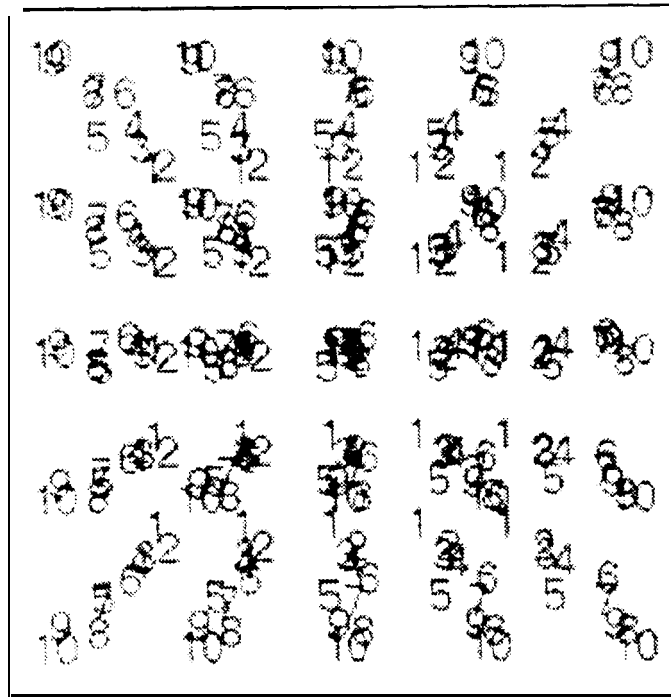
Tomographic reconstruction computations yield the spectrum for every pixel in the scene

Simulation of an Artificial Scene



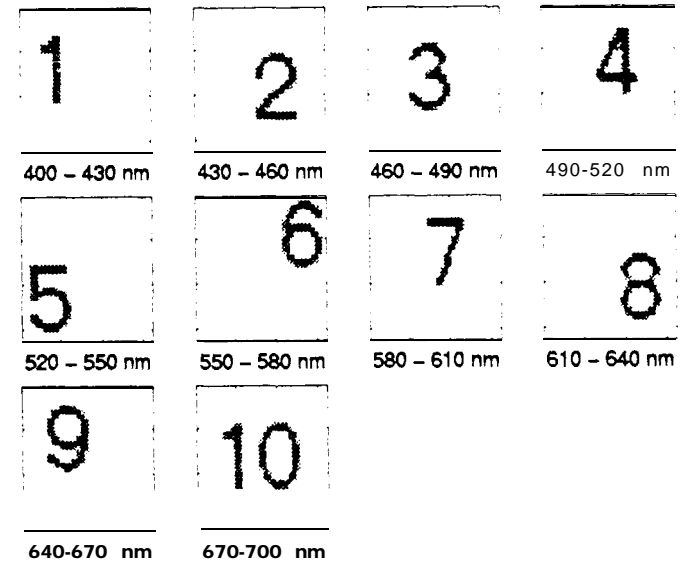
Multi-Spectral Scene

Scene traced through CTIS system having a 5x5-order disperser onto a 256x256-pixel focal plane array.



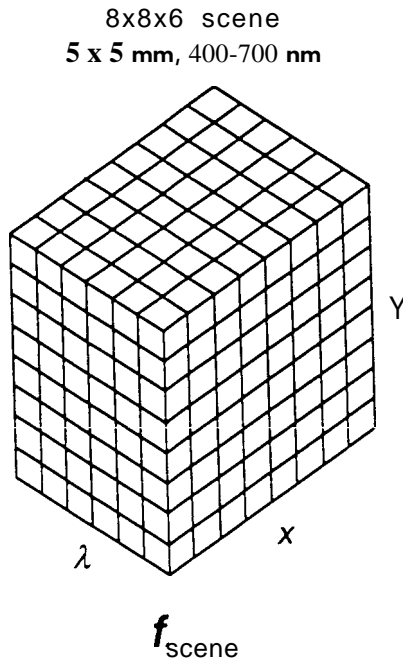
Black and White Focal Plane Array Intensity
256 X 256 CCD

•Spectral content in scene determined by tomographic reconstruction using focal plane array intensity and CTIS system matrix.

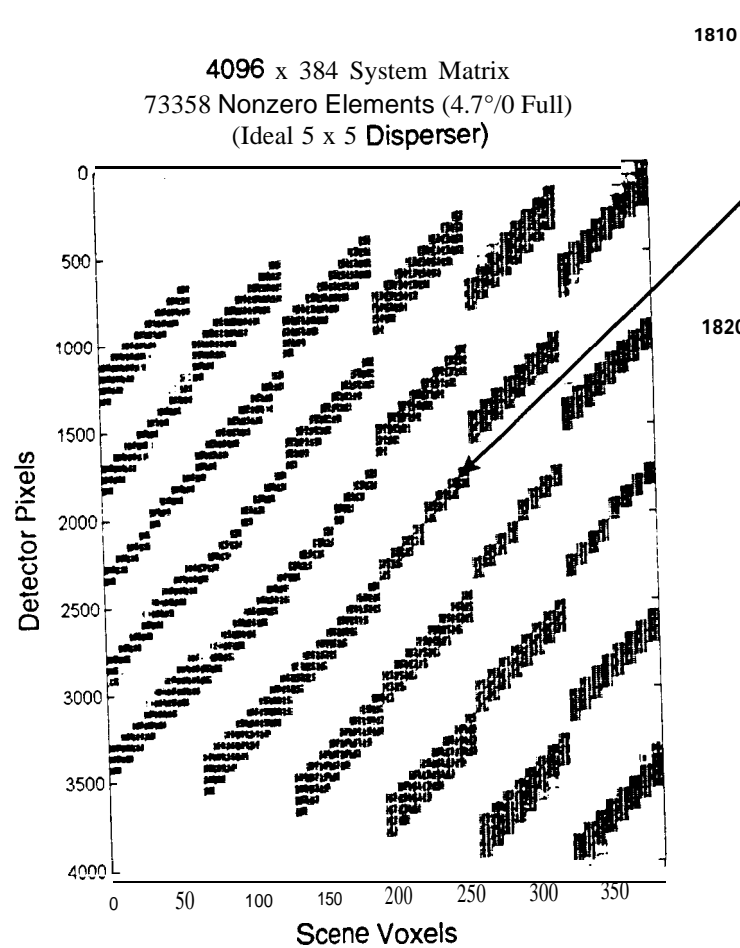


Reconstructed Spectral Images of Scene
Spatial Resolution: 32x 32

Calculation of System Matrix



- Scene represented as cube of 3D (x, y, λ) voxels
- Many rays traced from random positions inside each voxel through system to detector
- Measured order efficiencies used during ray tracing (includes spectral response of detector and transmission of any filters in system)



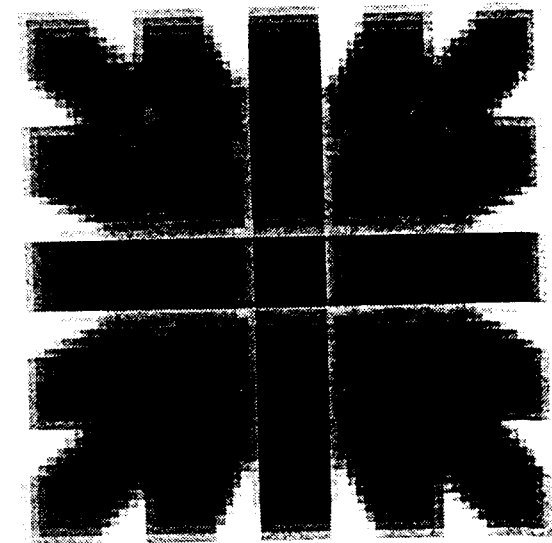
H_{Sys}

- System matrix gives the detector response (pixel intensity values) due to the scene voxels
- This matrix must be known to reconstruct an unknown scene from its detector response

1810	0.1076	0.2882	0	0
	0.2882	0.0104	0	0
	0.0174	0	0	0
	0	0	0	0
	0	0	0	0
	0	0	0	0.5139
	0	0	0.4236	2.5451
	0	0	2.5903	0.309C
	0	0	0.3611	(
	0	0	0	C
	0	0.0486	0	C
247				250

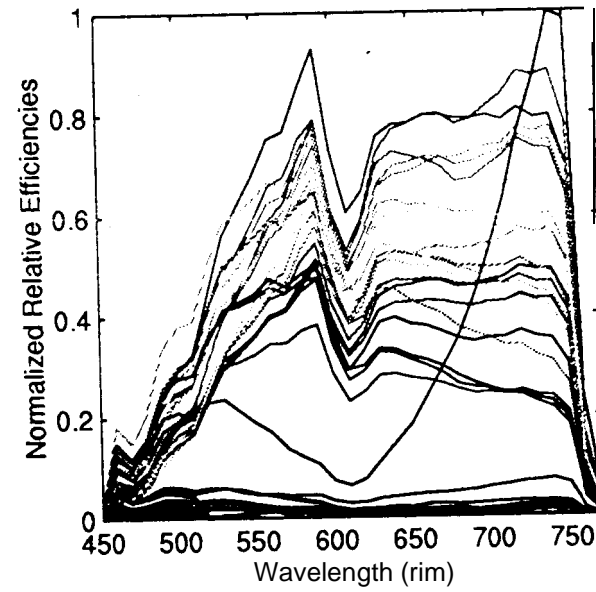
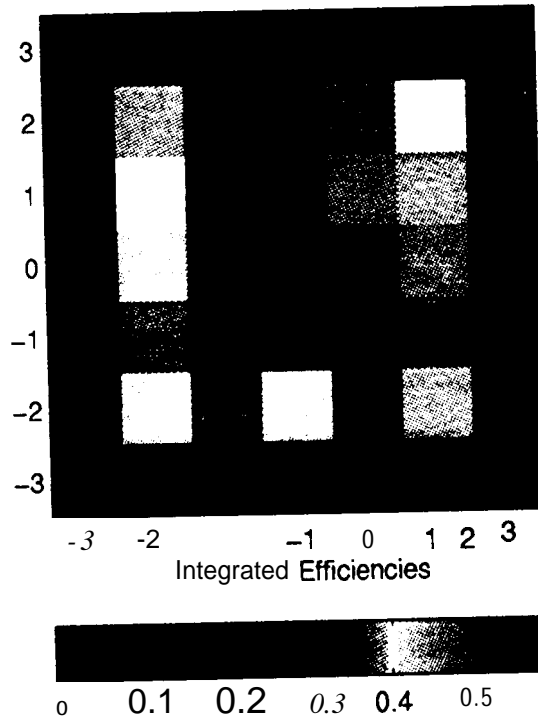
g_{det}

64 x 64 Detector



- Detector intensity after complete scene of unity strength voxels have been traced (uniform white scene)

Measured Diffraction Order Efficiencies (Field stop to FPA)



Tomographic Scene Reconstruction

- . CTIS system can be described by the equation

$$\mathbf{g}_{\text{det}} = \mathbf{H}_{\text{sys}} \mathbf{f}_{\text{scene}} + \mathbf{n}_{\text{noise}}$$

- . For reconstruction of the scene $\mathbf{f}_{\text{scene}}$ from the detector \mathbf{g}_{det} , utilize the Expectation Maximization algorithm from medical positron-emission tomography

Starts with a guess for the scene vector \mathbf{f}

Generates a predicted detector intensity \mathbf{g}

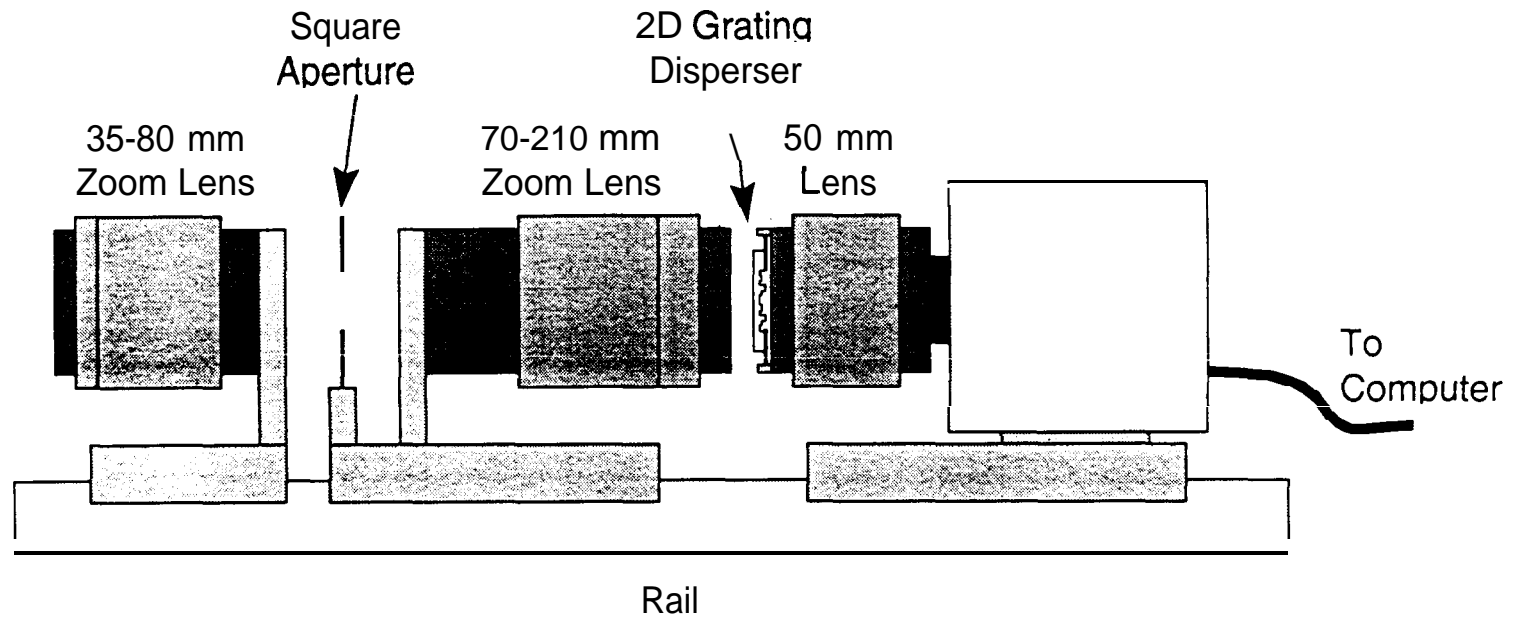
$$\mathbf{g}_{\text{det}} = \mathbf{H}_{\text{sys}} \mathbf{f}_{\text{scene}}$$

Makes corrections to the scene based on ratio between predicted and measured detector intensities

$$f'_s = f_s \left(\frac{1}{\sum_d H_{d,s}} \right) \left[\mathbf{H}^T \left(\frac{\mathbf{g}_{\text{meas}}}{\mathbf{g}_{\text{pred}}} \right) \right]_s, \quad s = 1 \dots N_s$$

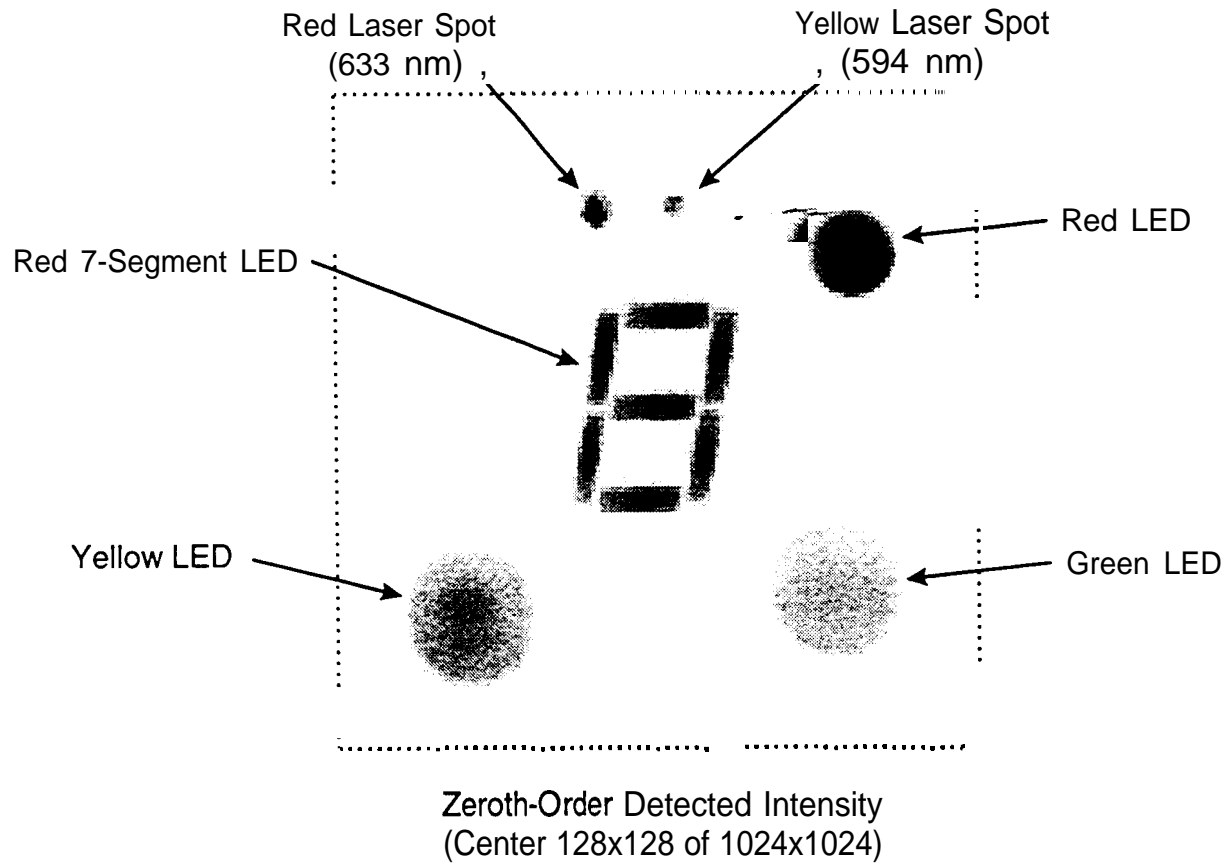
Iterates until predicted detector intensity matches the measured detector intensity to a desired tolerance

Bench-Top Experimental System

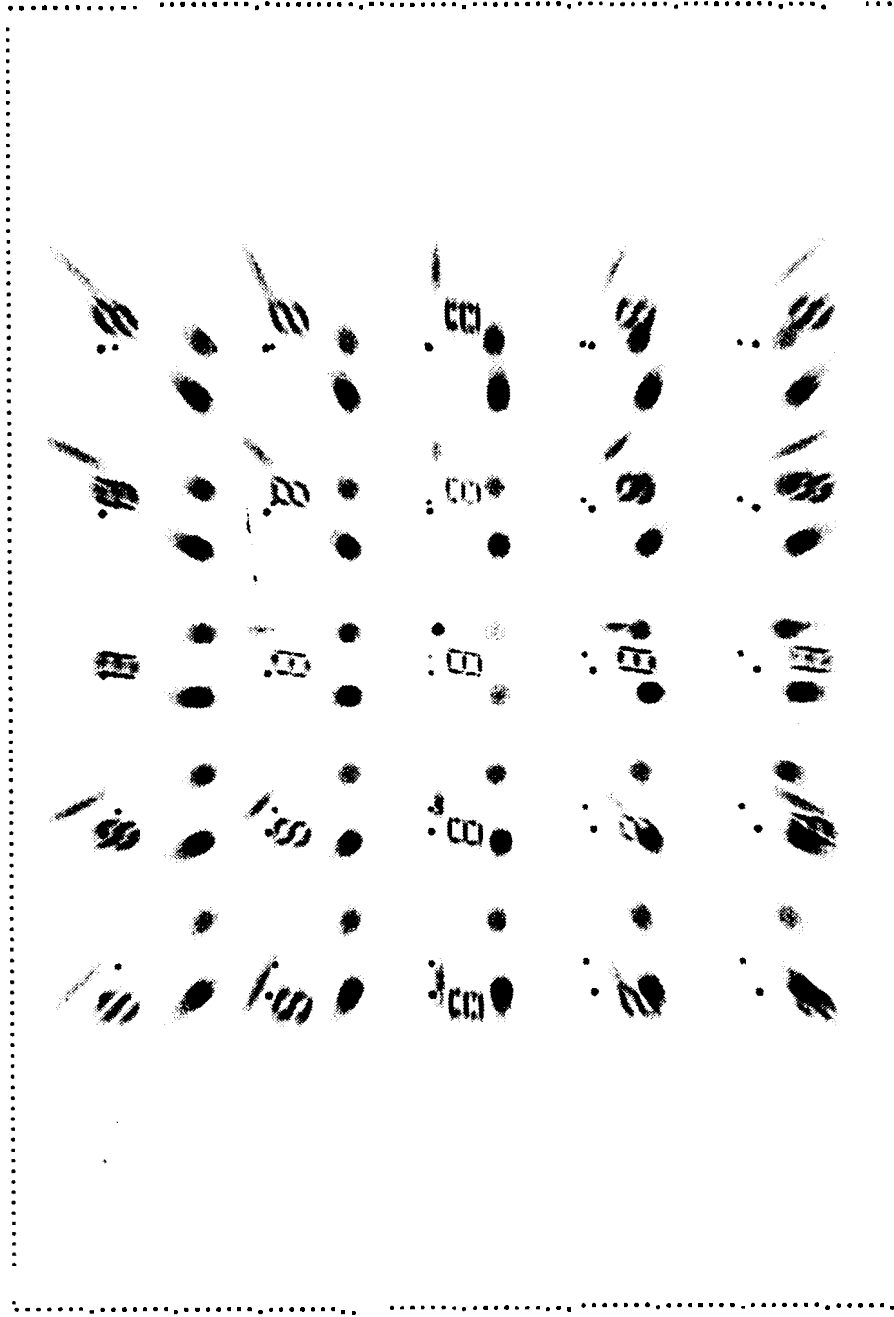


- . All commercial components, except E-beam fabricated disperser
- . High-resolution digital camera allows investigation of focal plane array requirements

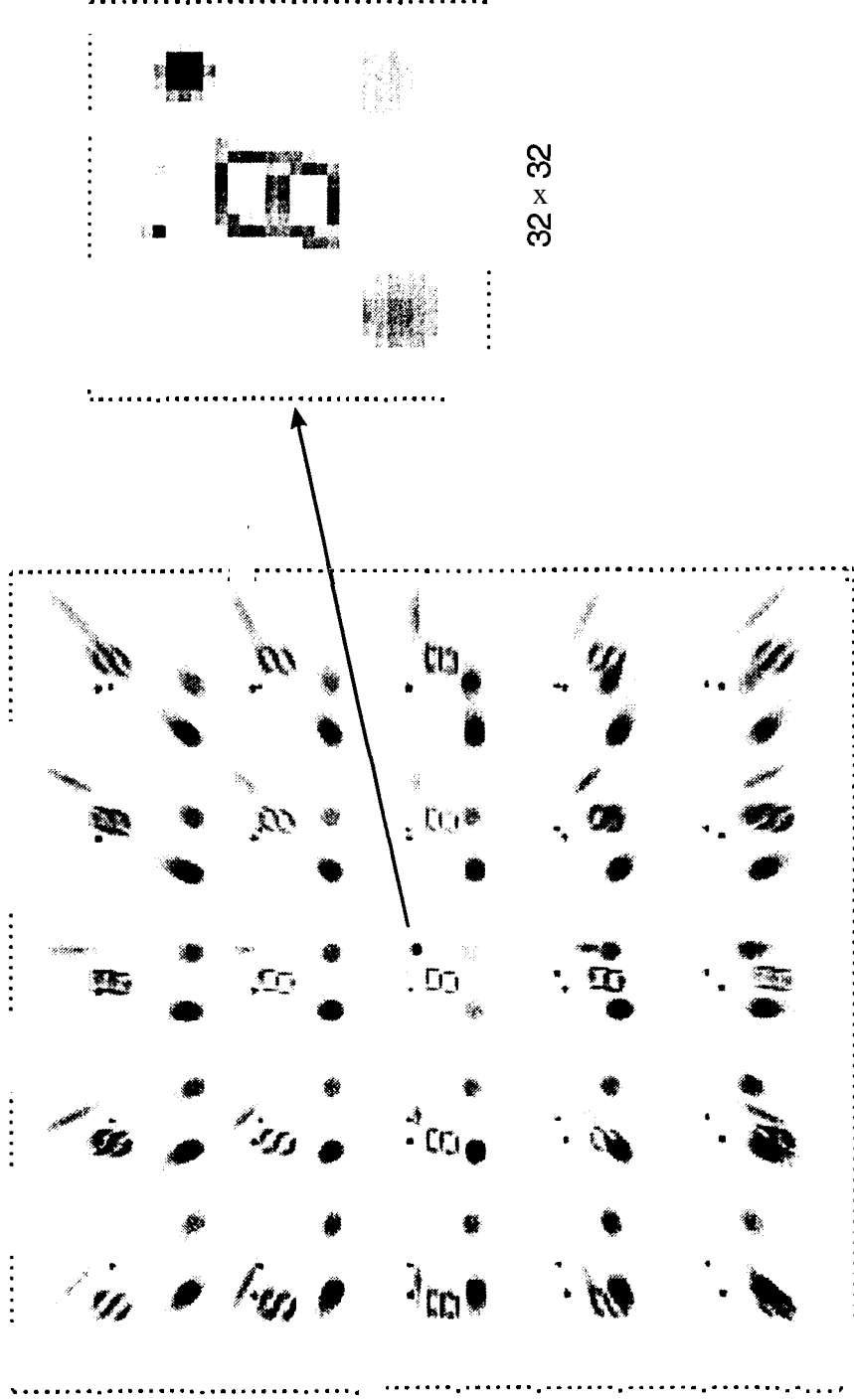
Experimental Scene



Full Resolution Detector (1024 x 1528)



Binned Detector Intensity used in Tomographic Reconstruction



256 x 256 = 65536 pixels

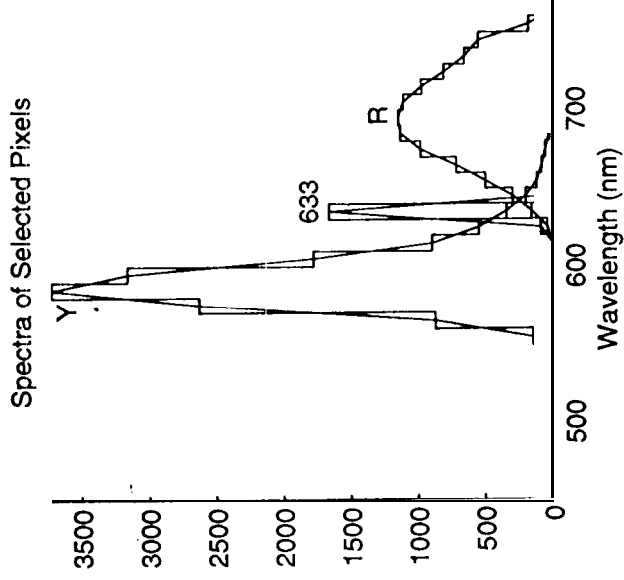
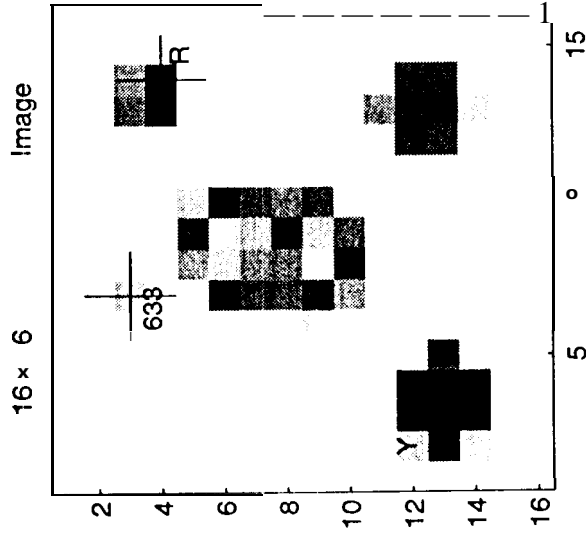
Reconstructions of Experimental Scene

Scene Resolution $N_x \times N_y \times N_z$ (450-770 nm)	Matrix Size	Nonzero Density	Storage (MB)	EM Time (see) (20 iterations)	Normalized Error
16x16x16	65536x4096	0.92 %	18.9	10.7	0.0112
16x16x32	65536x8192	0.64 %	26.3	15.0	0.0103
16x16x48	65536x12288	0.55 %	33.7	18.9	0.0103
32x32x16	65536x6384	0.51 %	41.8	22.5	0.0071
32x32x32	65536x32768	0.33 %	54.1	29.2	0.0042
32x32x48	65536x49152	0.27%	66.0	36.1	0.0041
40x40x32	65536x51200	0.28 %	72.0	37.6	0.0035
64x64x3	65536x12288	1.49 %	91.3	1957 (disk cached)	0.0336
40x40x8 unequal bands	65536x8192	0.75%	48.2	25.4	0.0109

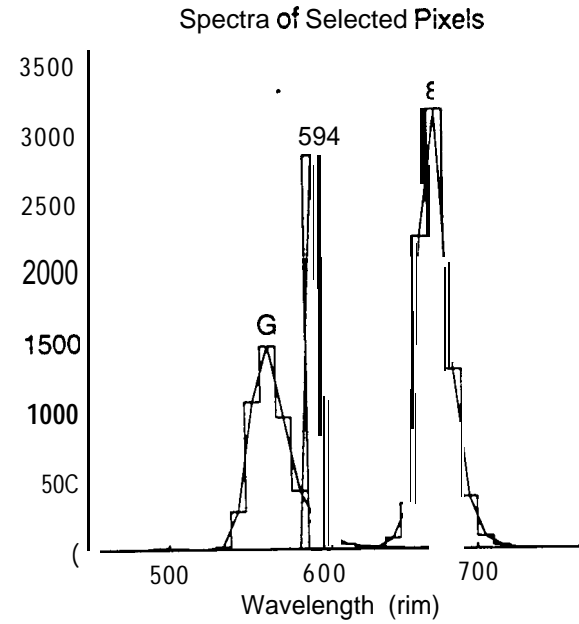
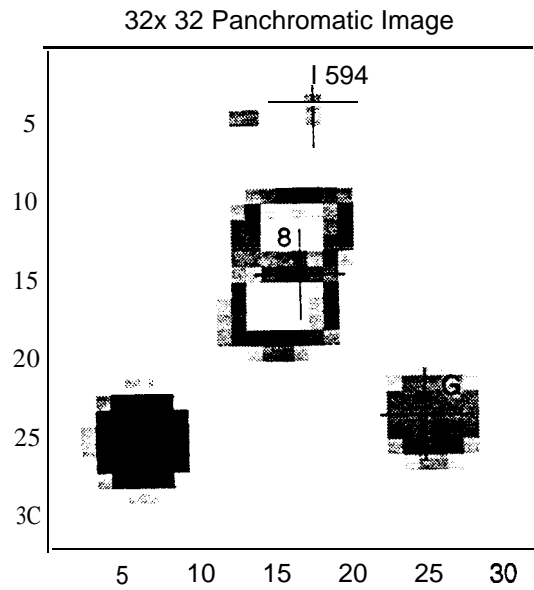
System Parameters: Field stop size = 4.5 mm, $f_1 = 210$ mm, $f_2 = 51.64$ mm, 2D Grating period = 19.2 μm

Detector size: 9.216x9.216 mm, 1024x1024 \sim m pixels binned 4x4 to 256x256 36- μm pixels

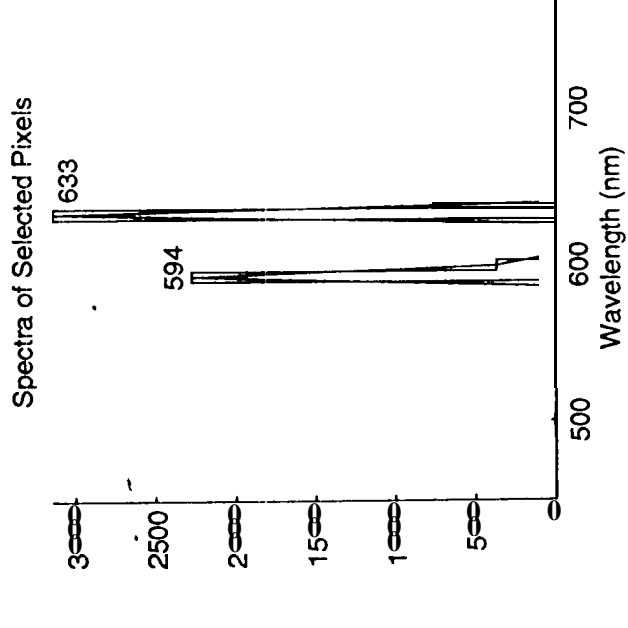
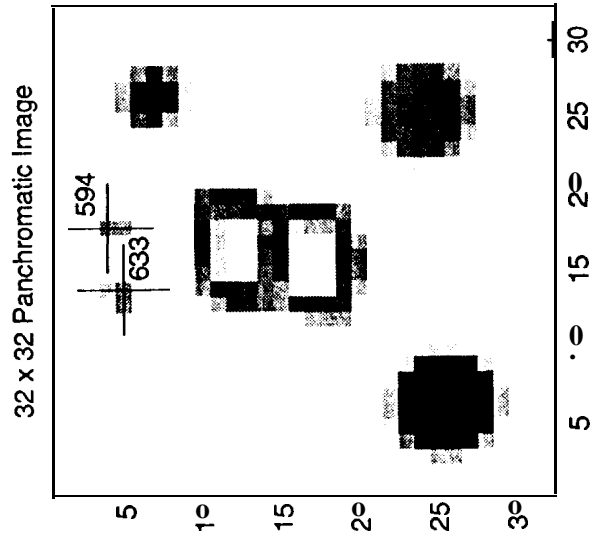
16 x 16 x 32 Reconstruction



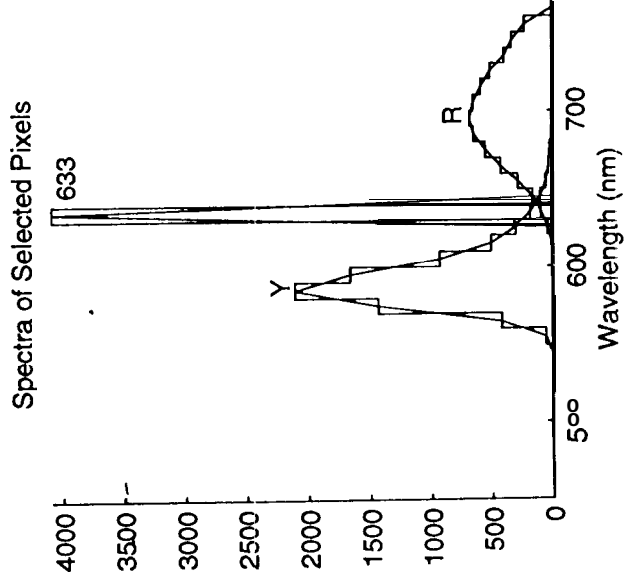
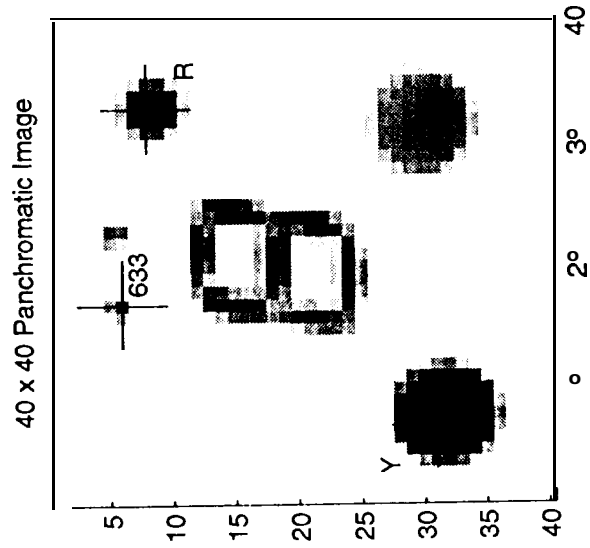
32x 32x 32 Reconstruction



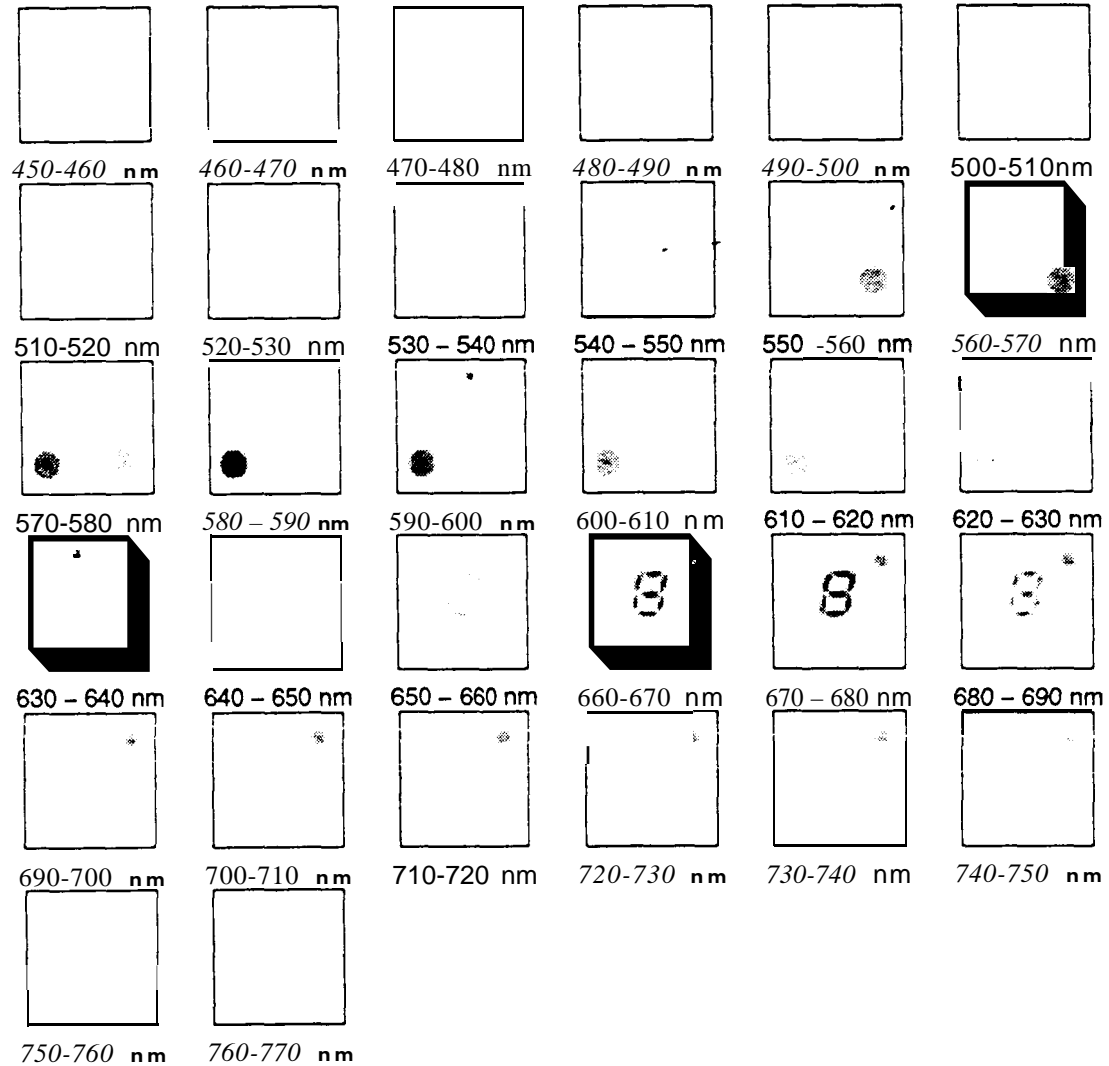
32 x 32 x 48 Reconstruction



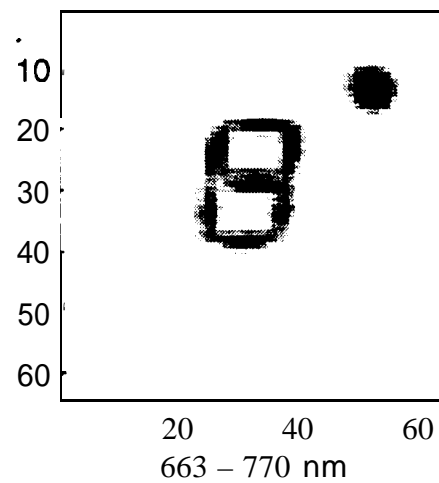
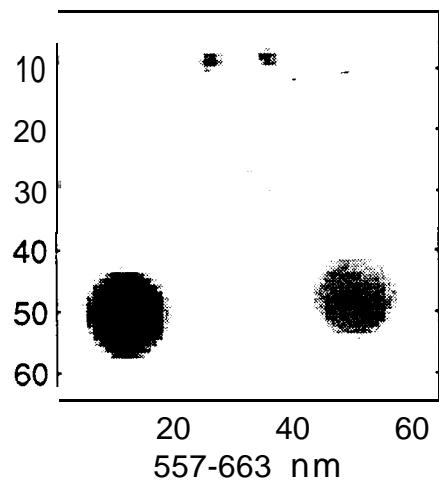
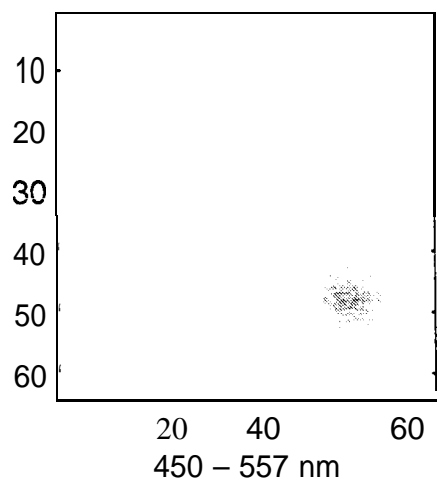
40 x 40 x 32 Reconstruction



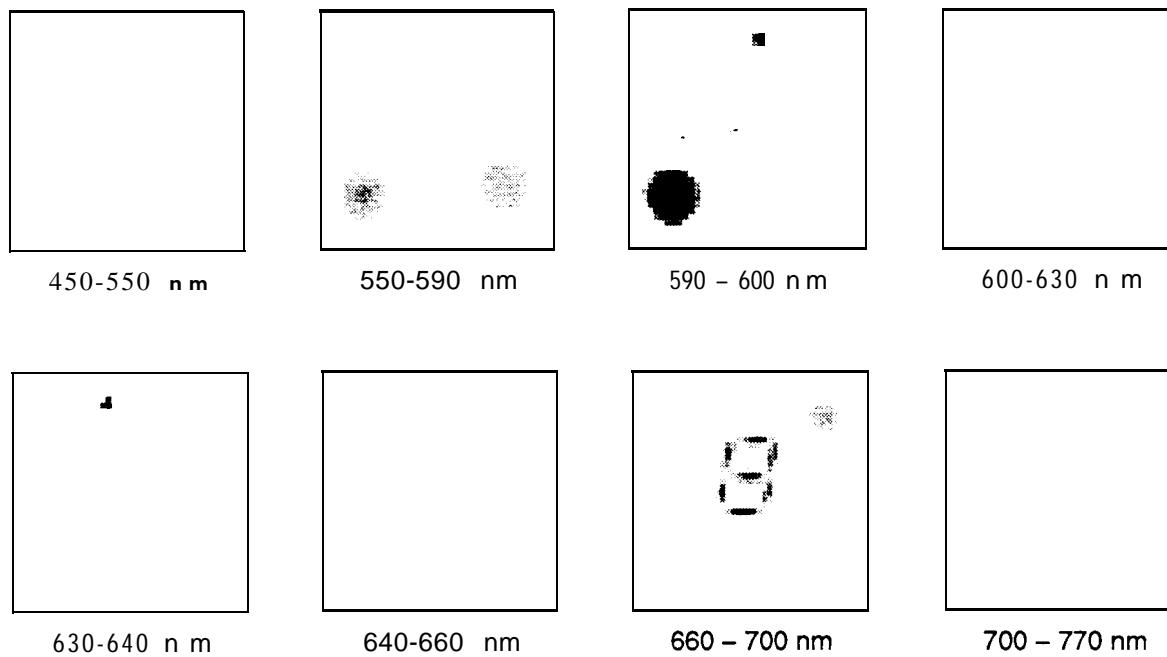
Reconstructed Scene (40 x 40 pixels x 32 bands)



64x 64x 3 Reconstruction



40x 40 x 8 Unequal Bands Reconstruction



Summary

- CTIS is does not employ scanning of any type. Captures a scene's spatial and spectral information in a single snapshot. Simple, robust, FPA camera system.
 - Transient events can be imaged without corrupting the data
- Single data set can be post-processed to yield different spatial or spectral resolutions
 - Same system can be used for multiple applications (high-spatial / low-spectral resolution or low-spatial / high-spectral resolution)
- Developed measurement+simulation calibration technique (measured spectral efficiencies and calculated imaging performance)

Comparison to calibrated point spectrometers needed for validation

Resolution can be adjusted after instrument deployment

Resolution need not be equal for all spectral bands/spatial elements